ACS OMEGA

http://pubs.acs.org/journal/acsodf

Article

Mapping the Interfacial Electronic Structure of Strain-Engineered Epitaxial Germanium Grown on $In_xAl_{1-x}As$ Stressors

Michael B. Clavel, Jheng-Sin Liu, Robert J. Bodnar, and Mantu K. Hudait*

Cite This: *ACS Omega* 2022, 7, 5946−5953

Read Online

ACCESS | Metrics & More | Article Recommendations

ABSTRACT: The indirect nature of silicon (Si) emission currently limits the monolithic integration of photonic circuitry with Si electronics. Approaches to circumvent the optical shortcomings of Si include band structure engineering via alloying (e.g., $Si_xGe_{1-x-y}Sn_y$) and/or strain engineering of group IV materials (e.g., Ge). Although these methods enhance emission, many are incapable of realizing practical lasing structures because of poor optical and electrical confinement. Here, we report on strong optoelectronic confinement in a highly tensile-strained (ε) Ge/$In_{0.26}Al_{0.74}As$ heterostructure as determined by X-ray photoemission spectroscopy (XPS). To this end, an ultrathin (∼10 nm) ε-Ge epilayer was directly integrated onto the $In_{0.26}Al_{0.74}As$ stressor using an in situ, dual-chamber molecular beam epitaxy approach. Combining high-resolution X-ray diffraction and Raman spectroscopy, a strain state as high as $\varepsilon \sim 1.75\%$ was demonstrated. Moreover, high-resolution transmission electron microscopy confirmed the highly ordered, pseudomorphic nature of the as-grown ε-Ge/$In_{0.26}Al_{0.74}As$ heterostructure. The heterointerfacial electronic structure was likewise probed via XPS, revealing conduction- and valence band offsets (ΔE_C and ΔE_V) of 1.25 ± 0.1 and 0.56 ± 0.1 eV, respectively. Finally, we compare our empirical results with previously published first-principles calculations investigating the impact of heterointerfacial stoichiometry on the ε-Ge/$In_xAl_{1-x}As$ energy band offset, demonstrating excellent agreement between experimental and theoretical results under an $As_{0.5}Ge_{0.5}$ interface stoichiometry exhibiting up to two monolayers of heterointerfacial As−Ge diffusion. Taken together, these findings reveal a new route toward the realization of on-Si photonics.

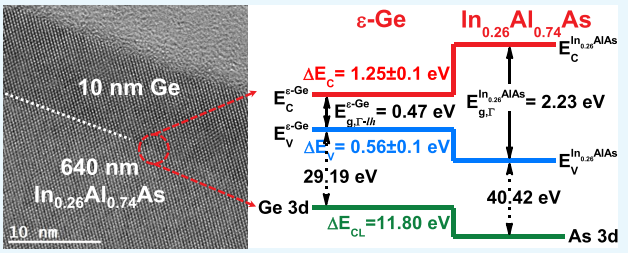

INTRODUCTION

With the increasing ubiquity of computing devices and the corresponding rise in bandwidth requirements, high-speed, large-bandwidth optical data transmission has been proposed as a cost-effective, low-loss solution for intra and interchip communication.[1−3] Consequently, extensive research has been conducted to realize the monolithic integration of photonic circuitry with state-of-the-art silicon (Si) electronics.[4−7] Although Si-based optoelectronics[8] offer a desirable solution because of the ease with which they can be integrated into current complementary metal-oxide-semiconductor process flows, the indirect bandgap of Si limits its radiative recombination efficiency and thus its suitability for on-chip light sources.[4] To overcome these challenges, researchers have focused on alternative integration approaches that employ direct or pseudodirect bandgap materials attained through band structure engineering,[9−11] strain engineering,[12−14] wafer bonding,[15−17] or novel lasing structures.[18] In particular, the band structure engineering of group IV-based elemental, binary, and ternary semiconductors (e.g., Ge, $Ge_{1-y}Sn_y$, $Si_xGe_{1-x-y}Sn_y$) has seen rapid progress, with recent demonstrations of Ge nanomembrane and microdisk light-emitting diodes and lasers,[19−21] laser structures fabricated from heavily doped and tensile-strained Ge directly grown on Si,[22,23] and $Ge_{1-y}Sn_y$ waveguide lasers.[24] Although several of these efforts have been successful in achieving enhanced emission from group IV, predominately Ge-based, materials,[19,21,24−26] none are compatible with the development of a group IV-based quantum well (QW) laser because of their inability to control optical and electronic confinement. Thus, the difficulty in realizing low-threshold current group IV-based QW lasers is twofold: (i) sufficient band structure and/or strain engineering must be introduced such that the emitting material is direct-gap in nature and (ii) sufficient optical and electronic confinement must be provided such that recombination is strictly limited to the gain medium.

To address these challenges, this work leverages the capacity of group IV/III−V heterostructures to impart modular, epitaxial stress on overlying group IV thin-films,[27−30] while simultaneously providing sufficient optical[18,31,32] and elec-

Received: November 4, 2021
Accepted: December 31, 2021
Published: February 8, 2022

tronic confinement[33] so as to realize practical lasing structures. Using solid-source molecular beam epitaxy (MBE), we demonstrate the low-defect, pseudomorphic epitaxy of a highly tensile-strained Ge (ε-Ge) epilayer on an $In_xAl_{1-x}As$ stressor. It is anticipated that such strain-engineered group IV materials could serve as the gain medium in future QW heterostructure lasers, whereas the high-bandgap $In_xAl_{1-x}As$ stressor could function as the cladding.[34] Moreover, characterization of the ε-Ge/$In_xAl_{1-x}As$ heterostructure material and electronic properties reveal energy band offsets (ΔE_C = 1.25 ± 0.1 eV; ΔE_V = 0.56 ± 0.1 eV) conducive to electro-optical confinement. Finally, we elucidate the role played by heterointerface stoichiometry in the interfacial energy band alignment through a comparison of our measured heterointerfacial electronic structure with that explored via extensive first-principles calculations reported in ref 35. Through the synthesis of our empirical findings with the reported ab initio modeling of the ε-Ge/$In_xAl_{1-x}As$ heterointerface, we provide a new route toward the realization of group IV-based photonic devices.

RESULTS AND DISCUSSION

Strain and Structural Characterization of the ε-Ge/$In_xAl_{1-x}As$ Heterostructure. Figure 1a presents a cross-sectional schematic diagram of the ε-Ge/$In_{0.26}Al_{0.74}As$ heterostructure investigated in this work. As demonstrated in Figure 1b, epitaxially induced biaxial tensile stress results in an expanded in-plane lattice constant ($a_\parallel$) and compressed out-of-plane lattice constant ($a_\perp$) within the overlying epilayer. For strained epilayer thicknesses below the critical layer thickness (h_c), it is expected that the strained layer and stressor in-plane lattice constants will be lattice-matched, that is, $a_{\parallel,\text{epilayer}} = a_{\parallel,\text{stressor}}$. Correspondingly, the optical and electronic properties of the overlying strained layer can be tuned within a wide range by tailoring the InAs molar fraction of an $In_xAl_{1-x}As$ stressor to vary the stressor lattice constant (a_{AlAs} = 5.661 Å ≤ $a_{InxAl1-xAs}$ ≤ a_{InAs} = 6.0583 Å) and therefore the epitaxial strain ($\varepsilon_{Ge/AlAs}$ = +0.05% ≤ ε ≤ $\varepsilon_{Ge/InAs}$ = +7.07%).

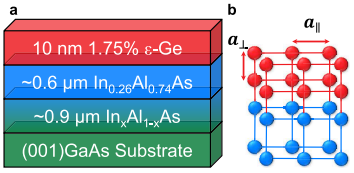

Figure 1. (a) Cross-sectional schematic diagram of the ε-Ge/$In_{0.26}Al_{0.74}As$ heterostructure grown on (001)GaAs. (b) Graphic representation of the influence of biaxial tensile stress on the in-plane ($a_\parallel$) and out-of-plane ($a_\perp$) lattice constants of a pseudomorphic thin film (red) grown onto a lattice-mismatched stressor (blue).

For this study, a target InAs molar fraction of 0.25 was chosen, corresponding to a nominal ∼1.8% tensile strain with respect to the relaxed Ge lattice constant. Such a relatively high Ge strain state was selected to increase the likelihood of direct-gap recombination within the Ge epilayer (gain medium), prompted by a reduction in the ε-Ge Γ-valley conduction band minimum (CBM) by ∼26 meV below that of the L-valley CBM.[36,37] Likewise, the Ge epilayer thickness (10 nm) was determined so as to reduce the likelihood of strain relaxation within the Ge thin-film (h_c ∼ 30 nm).[29] High-resolution X-ray diffraction (HR-XRD) data of the as-grown heterostructure reveal that the Ge epilayer was indeed pseudomorphic with respect to the underlying $In_xAl_{1-x}As$ stressor. Figure 2a,b shows the symmetric (004) and asymmetric (115) RSMs, respectively, recorded from the ε-Ge/$In_xAl_{1-x}As$ heterostructure. We note that the reciprocal lattice contour (RLC) centroid for each epilayer has been highlighted for clarity. As can be seen from the symmetric (004) RSM shown in Figure 2a, the strain-induced compression of $a_{\perp,Ge}$ was observed directly as a modification to the (004) Bragg angle of the ε-Ge film, and thus, a corresponding change in the Q_z component of the ε-Ge RLC. Further examination of the asymmetric (115) RSM (Figure 2b) revealed a close alignment in the Q_x components of the ε-Ge and $In_xAl_{1-x}As$ RLCs, indicative of coherent strained layer epitaxy.[38] Moreover, the Q_x−Q_z symmetry of the ε-Ge RLC suggested a uniform crystallinity absent of substantial mosaicity-inducing crystal defect scattering. By the same token, the relatively low Bragg diffraction intensity of the Ge epilayer can be ascribed to its minute diffraction volume, as opposed to crystal defect-induced scattering. Similarly, the narrow and symmetric nature of the $In_xAl_{1-x}As$ stressor RLC suggested a strong confinement of lattice mismatch-induced defects within the metamorphic linearly graded $In_xAl_{1-x}As$ buffer, thereby minimizing dislocation propagation into the $In_{0.26}Al_{0.76}As$ stressor and hence, the active region (cladding). To quantify these observations, the measured RSM data were used to determine $a_\parallel$, $a_\perp$, and ε for the ε-Ge epilayer, as well as the InAs molar fraction of the $In_xAl_{1-x}As$ stressor, following the procedures outlined in ref 38. Defining the in-plane epitaxial strain to be

$$\varepsilon = \frac{a_\parallel - a_r}{a_r} \quad (1)$$

where $a_\parallel$ and a_r correspond to the in-plane and relaxed epilayer lattice parameters, respectively, and the strain state of the ε-Ge epilayer was found to be ε = 1.76% utilizing the literature value of 5.658 Å for the relaxed Ge lattice constant[39] and the measured value of 5.7578 Å for $a_\parallel$ ($a_\perp$ = 5.6051 Å). We note that the experimental $In_xAl_{1-x}As$ stressor InAs molar fraction (x_{exp} ∼ 0.26) was slightly higher than the targeted value (x_{ideal} = 0.25), which was attributed to the competing add-atom surface mobilities of In and Al dimers. Additionally, the $In_{0.26}Al_{0.74}As$ stressor was found to be over 90% relaxed. From the 306 arcsec tilt measured along the (004) reflection, it can be posited that buffer relaxation occurred in a predominately symmetric nature, with only a minimal amount of observable anisotropy stemming from the disparity between α (group V-terminated core) and β (group III-terminated core) dislocation glide velocities oriented along the $\langle 1\bar{1}0\rangle$ and $\langle 110\rangle$ orthogonal directions, respectively.[40]

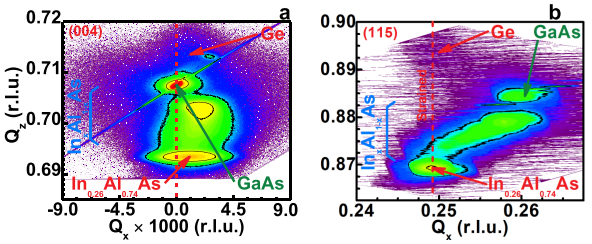

Figure 2. High-resolution reciprocal space maps (RSMs) taken along (a) symmetric (004) and (b) asymmetric (115) crystallographic orientations. The separation between the Ge reciprocal lattice point and that of the substrate (GaAs) in the Q_z coordinate is indicative of compressive out-of-plane stress and thus tensile in-plane stress.

https://doi.org/10.1021/acsomega.1c06203
ACS Omega 2022, 7, 5946−5953

Atomic force microscopy (AFM) analysis of the as-grown ε-Ge/$In_{0.26}Al_{0.74}As$ surface (Figure 3) provided ancillary support

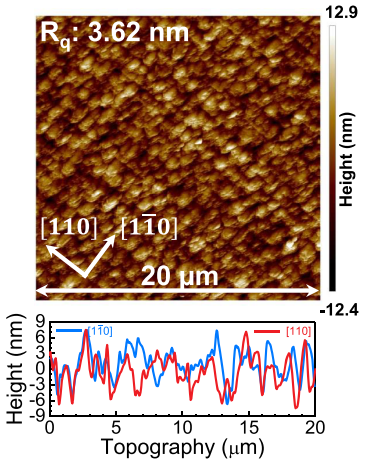

Figure 3. Atomic force micrograph of a representative 20 μm × 20 μm region of the as-grown ε-Ge/$In_{0.26}Al_{0.74}As$ surface and related line height profiles recorded along the two orthogonal ⟨110⟩ symmetric directions.

for this conclusion, wherein the observed symmetric cross-hatch surface morphology was indicative of predominantly isotropic buffer relaxation. The relatively low measured rms surface roughness ($R_q \sim 3.62$ nm) was mirrored, with minimal deviation, along both ⟨1$\bar{1}$0⟩ and ⟨110⟩ orthogonal directions, from which the orientation-dependent R_q values of 3.30 and 3.41 nm, respectively, were obtained. It is well known[29] that the uniformity of the surface topography can be directly correlated with the extent of (an)isotropic strain relaxation present in a film(s). This is a result of the origins of the cross-hatch morphology, wherein plastic relaxation processes within the growing film preferentially create dislocations within the (energetically favorable) $a/2\langle 110\rangle\{111\}$ slip system. The successive process of strained film growth and relaxation, such as that which occurs in a metamorphic buffer, propagates surface morphology vertically via the formation of hillocks and valleys oriented along dislocation lines. As defects (threading and misfit dislocations) propagate laterally along ⟨110⟩ directions, analysis of the AFM surface morphology of a heterostructure can hence provide indirect evidence for the relaxation mechanism(s) present during epitaxy. It is within this lens that one can relate the uniform, cross-hatched surface of Figure 3 to the HR-XRD-derived tilt (306 arcsec), suggesting that the two-step $In_xAl_{1-x}As$ metamorphic buffer strategy successfully balanced the competing In and Al add-atom surface mobilities during buffer growth. Moreover, given the ultrathin character of the ε-Ge epilayer (t_{Ge} = 10 nm), it is unlikely that subsequent ε-Ge epitaxy would quantitatively alter the $In_{0.26}Al_{0.74}As$ stressor surface morphology provided that the ε-Ge epilayer remained pseudomorphic.

To this end, Raman spectroscopic data (Figure 4) further confirmed the nature of the ε-Ge epilayer strain, as demonstrated by the frequency shift observed in the measured ε-Ge/$In_{0.26}Al_{0.74}As$ Raman spectra. Explicitly, when a biaxial strain is applied to a (001) oriented diamond-cubic crystal, the threefold degenerate zone-center optical phonon modes are split into a doublet and singlet having eigenvectors perpendicular and parallel to the plane, respectively.[41] Consequently, considering the (001) backscattering geometry

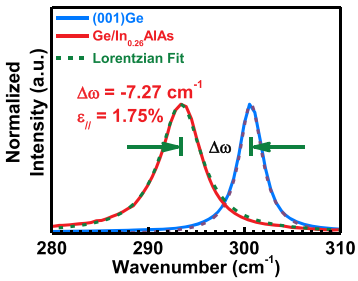

Figure 4. Raman spectra collected from a (001)Ge substrate and the ε-Ge epilayer grown on $In_{0.26}Al_{0.74}As$. The shift ($\Delta\omega = -7.27$ cm^{-1}) in the unstrained Ge LO-related mode ($\omega_0 \sim 300$ cm^{-1}) corresponds to an in-plane strain of 1.75%.

used in this work, application of the selection rules provided in ref[41] implies that solely the longitudinal optical (LO) mode corresponding to the singlet is experimentally observable. Additionally, the inclusion of a lattice strain produces a hydrostatic shift of the phonon frequency (Ω_S) and therefore a relative shift in the measured Raman wavenumber ($\Delta\omega$) with respect to its relaxed value (ω_0). Thus, the strain state of a material and the type of strain present are directly correlated with the magnitude and sign of the wavenumber shift, for example, a positive (negative) $\Delta\omega$ corresponds to compressive (tensile) stress.

As shown in Figure 4, the ε-Ge epilayer demonstrated a wavenumber shift of −7.27 cm^{-1} with respect to the Raman spectra recorded from a (001)Ge substrate. Previously,[42,43] we have utilized the relation $\Delta\omega = -b\varepsilon_{\parallel}$ to analyze the Raman shift as a function of strain ($\varepsilon_{\parallel} \leq 2.0\%$) in ε-Ge epilayers grown on (001)GaAs and (001)Si substrates, wherein $\Delta\omega$ is the measured wavenumber shift, $\varepsilon_{\parallel}$ is the in-plane strain, and b is a material parameter dependent on the phonon deformation potentials, elastic constants, and unstrained phonon frequency ($\omega_0 \sim 300$ cm^{-1} for Ge) of the material. Using a value of −415 for b,[27] the Raman-deduced in-plane strain was found to be ε = 1.75%, in good agreement with both the theoretical misfit ($f \sim 1.8$) and the strain determined via X-ray diffraction (ε_{XRD} = 1.76%).

Finally, to gain further insight into the material and structural properties of the ε-Ge/$In_xAl_{1-x}As$ heterostructure, low- and high-magnification cross-sectional micrographs from representative growth regions were captured via transmission electron microscopy (TEM). Figure 5a,b shows the low- and high-magnification bright-field TEM micrographs corresponding to the complete heterostructure and the ε-Ge/$In_{0.26}Al_{0.74}As$

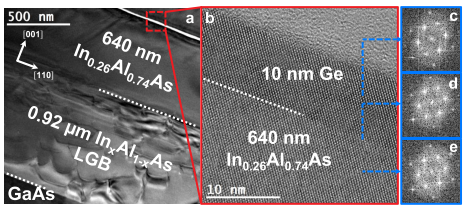

Figure 5. (a) Low-magnification cross-sectional transmission electron micrograph (X-TEM) of the entire ε-Ge/$In_xAl_{1-x}As$/GaAs heterostructure, highlighting the confinement of lattice mismatch-induced defects below the region of interest. (b) and (c−e) High-magnification X-TEM of the ε-Ge/$In_{0.26}Al_{0.74}As$ heterointerface and associated FFT patterns, respectively, revealing coherent strained-layer epitaxy with no observable relaxation-induced interface defects.

https://doi.org/10.1021/acsomega.1c06203
ACS Omega 2022, 7, 5946−5953

heterointerface, respectively. As can be seen from Figure 5a, the metamorphic linearly graded $In_xAl_{1-x}As$ buffer accommodated misfit strain (i.e., lattice mismatch) via the formation and subsequent glide of threading dislocations, thereby inhibiting substantial defect propagation along the growth axis. Correspondingly, the constant-composition $In_{0.26}Al_{0.74}As$ stressor was observed to be absent of long-range microstructural defects or disorder, implicitly reinforcing the high degree of relaxation and crystallinity found via XRD analysis. Examining Figure 5b, one can find that the epitaxial Ge and $In_{0.26}Al_{0.74}As$ strain template exhibited a highly uniform heterointerface. Moreover, further inspection utilizing a two-step Fast Fourier Transform (FFT) noise filtering approach (i.e., $\mathcal{F}^{-1}(\mathcal{F}(k))$) suggested an atomically abrupt heterointerface lacking substantive relaxation-inducing misfit dislocations. This conclusion was reinforced by the indistinguishable nature of FFT patterns taken from representative 6 nm × 6 nm regions of the (i) $In_{0.26}Al_{0.74}As$ strain template (Figure 5c), (ii) Ge/$In_{0.26}Al_{0.74}As$ heterointerface (Figure 5d) and (iii) epitaxial Ge layer (Figure 5e). The absence of satellite reflections in Figure 5c,d indicated the contribution of a single lattice parameter (i.e., $a_{In0.26Al0.74As} = a_{Ge}$) to the diffractogram, thereby reaffirming the pseudomorphic nature of the Ge epilayer as previously determined via HR-XRD and Raman spectroscopic analysis.

ε-Ge/$In_xAl_{1-x}As$ Heterointerface Band Alignment. Having demonstrated the feasibility of strained-layer Ge epitaxy on a large-bandgap (i.e., $In_xAl_{1-x}As$) stressor, we now address the nature of the energy band alignment at the Ge/$In_xAl_{1-x}As$ heterointerface. To this end, X-ray photoemission spectra were collected from three sample surfaces: (i) the 10 nm ε-Ge epilayer; (ii) the $In_{0.26}Al_{0.74}As$ stressor; and (iii) the heterointerface between ∼1.5 nm ε-Ge and the $In_{0.26}Al_{0.74}As$ stressor. We note that surfaces (ii) and (iii) were realized via the in situ sputtering of (i) by low-energy (≤1 kV) Ar^+ ion bombardment. Figure 6a−c shows representative spectra recorded from each sample surface, respectively, wherein spectral fitting using a Lorentzian peak convolution of the spin-orbit coupled core levels (CLs) yielded the binding energy (E_B) positions for the Ge $3d_{5/2}$ ($E^{\varepsilon-Ge}_{Ge\ 3d_{5/2}}$) and As $3d_{5/2}$ ($E^{In_{0.26}Al_{0.74}As}_{As\ 3d_{5/2}}$) states.

Likewise, the valence band maximum (VBM) binding energy for each material ($E^{\varepsilon-Ge}_{VBM}$ and $E^{In_{0.26}Al_{0.74}As}_{VBM}$) was determined by linearly fitting the onset of photoemission from the valence band density of states with respect to the experimental emission floor (inset of Figure 6a,b). Following the procedure introduced by Kraut et al., the valence band offset (ΔE_V) can be expressed as,[44]

$$\Delta E_V = (E_{Ge\ 3d_{5/2}} - E_{VBM})^{\varepsilon-Ge} - (E_{As\ 3d_{5/2}} - E_{VBM})^{In_{0.26}Al_{0.74}As} - (E^{In_{0.26}Al_{0.74}As}_{As\ 3d_{5/2}} - E^{\varepsilon-Ge}_{Ge\ 3d_{5/2}})^{i} \quad (2)$$

where $(E_{Ge(As)\ 3d_{5/2}} - E_{VBM})^{\varepsilon-Ge\ (In_{0.26}Al_{0.74}As)}$ is the binding energy separation between the Ge (As) $3d_{5/2}$ state and the VBM of the respective material and $(E^{In_{0.26}Al_{0.74}As}_{As\ 3d_{5/2}} - E^{\varepsilon-Ge}_{Ge\ 3d_{5/2}})^{i}$ is the binding energy separation between the Ge and As $3d_{5/2}$ states measured at the interface. Using the experimental binding energy separations of 29.19 ± 0.05, 40.42 ± 0.05, and 11.80 ± 0.05 eV, respectively, the corresponding ΔE_V at the ε-Ge/$In_{0.26}Al_{0.74}As$ heterointerface was found to be 0.56 ± 0.1 eV. Similarly, the conduction band offset (ΔE_C) can be derived as[44]

$$\Delta E_C = E_g^{In_{0.26}Al_{0.74}As} - E_g^{\varepsilon-Ge} - \Delta E_V \quad (3)$$

where $E_g^{In_{0.26}Al_{0.74}As}$ and $E_g^{\varepsilon-Ge}$ are the bandgaps of $In_{0.26}Al_{0.74}As$ and ε-Ge, respectively, and ΔE_V is the measured valence band offset. Using the calculated $In_{0.26}Al_{0.74}As$ and ε-Ge bandgaps of 2.23 eV[45] and 0.47 eV,[42,43] respectively, a value of 1.25 ± 0.1 eV was found for ΔE_C. Figure 6d summarizes these parameters in schematic form, illustrating a flat-band representation of the empirical Γ-valley energy band alignment at the ε-Ge/$In_{0.26}Al_{0.74}As$ heterointerface and highlighting the strong confinement to be expected in the ε-Ge epilayer. In the following section, we will correlate these empirical data with first-principles calculations of the electronic structure of ε-Ge/$In_xAl_{1-x}As$ heterojunctions[35] and, in so doing, elucidate the nature of the bonding environment and stoichiometry at the experimental ε-Ge/$In_{0.26}Al_{0.74}As$ heterointerface reported herein.

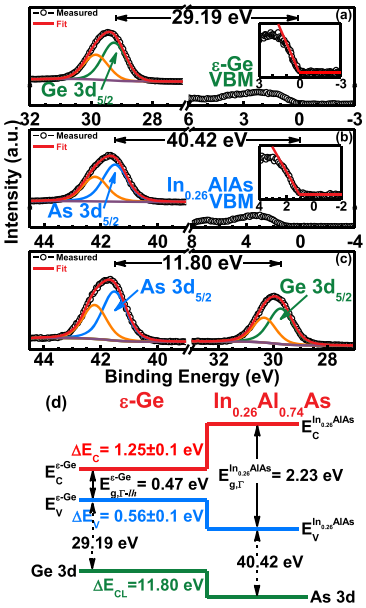

Figure 6. X-ray photoelectron spectroscopy (XPS) spectra of (a) Ge 3d CL ($E^{\varepsilon-Ge}_{Ge\ 3d}$) and valence band maximum ($E^{\varepsilon-Ge}_{VBM}$) from the ε-Ge thin-film, (b) As 3d ($E^{In_{0.26}Al_{0.74}As}_{As\ 3d}$) and VBM ($E^{In_{0.26}Al_{0.74}As}_{VBM}$) from the $In_{0.26}Al_{0.74}As$ stressor, and (c) As 3d and Ge 3d CLs measured at the ε-Ge/$In_{0.26}Al_{0.74}As$ heterointerface. (d) Schematic flat-band diagram for the ε-Ge/$In_{0.26}Al_{0.74}As$ heterostructure illustrating the relatively large valence (ΔE_V = 0.56 ± 0.1 eV) and conduction (ΔE_C = 1.25 ± 0.1 eV) band offsets found in this work.

Comparison of Empirical and Calculated Interfacial Electronic Structures. It has been well established that atomic interdiffusion across semiconductor heterojunctions is capable of quantitatively modifying the heterointerfacial energy band alignment,[46−52] wherein variations in the local bonding environment at the interface can correspond to a significant range of possible interfacial electronic configurations. This is particularly true for IV/III−V heterointerfaces, more specifically, Ge/III−V heterointerfaces, which have been predicted to exhibit either staggered (type I) or straddling (type II) interfacial electronic structures depending on the heterointerfacial stochiometry.[31,35] Despite this remarkable result, relatively few studies have been reported on the experimen-

https://doi.org/10.1021/acsomega.1c06203
ACS Omega 2022, 7, 5946−5953

tal[29,42,54] or theoretical[31,35] investigation of the heterovalent Ge/III−V interface. In particular, the first-principles-based systematic investigation of the heterovalent ε-Ge/$In_xA_{1-x}As$ interface by Greene-Diniz et al.[35] remains the only reported theoretical inquiry into the ε-Ge/$In_xAl_{1-x}As$ interfacial electronic structure, that is, the same property of the ε-Ge/$In_xAl_{1-x}As$ material system studied in this work. In ref 35, Greene-Diniz and co-workers employed density functional theory, utilizing the GW approximation, to calculate the ε-Ge/$In_xAl_{1-x}As$ interfacial electronic structure under abrupt and nonabrupt conditions. Expanding upon the latter, the ε-Ge/$In_xAl_{1-x}As$ heterointerface was then probed considering: (i) variations in the stoichiometry of a mixed interfacial region; (ii) variations in the InAs molar fraction (up to $x = 0.25$) of the $In_xAl_{1-x}As$ stressor; and (iii) interdiffusion of atomic species across the heterointerface, as well as their relative stability in the extrinsic material.[53]

A key finding of these investigations is highlighted in Figure 7, which graphically depicts the modification of the ε-Ge/$In_xAl_{1-x}As$ energy band alignment as a function of As updiffusion length into a strained ($\varepsilon \sim 1.76\%$) Ge epilayer overlying an As-terminated $In_{0.25}Al_{0.75}As$ stressor. We note that monolayer 0 (ML0) corresponds to an abrupt heterointerface with a singular mixed monolayer bridging the two disparate materials. Likewise, ML1 and ML2 correspond to the distance between the maximum extent of diffusion and the abrupt heterointerface, in monolayers; that is, the furthest such mixed monolayer from the abrupt interface case. The stoichiometry of these mixed monolayers is modeled as an equal number of As and Ge atoms, that is, $As_{0.5}Ge_{0.5}$, based on previous correlations between theoretical and empirical data from the lattice-matched Ge/AlAs(001) heterointerface.[54] As shown in Figure 7, an increase in updiffusion of As atoms (into the epitaxial Ge layer) corresponded to a substantial decrease in ΔE_V from 0.86 eV (in the abrupt case) to 0.48 eV (in the two-monolayer diffuse case, ML2). Utilizing the ab initio calculated bandgaps for 1.76% ε-Ge (0.43 eV) and $In_{0.25}Al_{0.75}As$ (2.05 eV), Greene-Diniz et al.[35] determined a concomitant increase in ΔE_C from 0.75 to 1.15 eV.

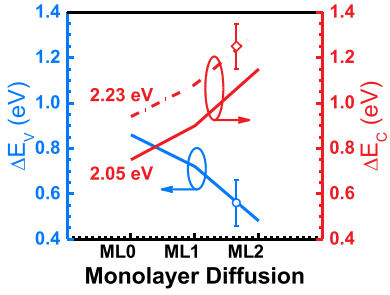

Figure 7. Calculated valence band offset (ΔE_V, left, blue) and conduction band offset (ΔE_C, right, red) as a function of arsenic (As) diffusion length into a ε-Ge epilayer overlying an As-terminated $In_{0.25}Al_{0.75}As$ stressor. Solid lines have been adapted from ref 35, whereas dashed lines represent ΔE_C when recalculated using the $In_xAl_{1-x}As$ bandgap provided in ref 45. Symbols (and associated error) correspond to the experimental energy band offsets as determined via XPS and reported in this work. The experimental data (symbols) were overlaid with the modeled "trend" (lines) to approximate the extent of As diffusion in the as-grown (empirical) ε-Ge/$In_{0.26}Al_{0.74}As$ heterostructure studied herein.

Comparing these data with the energy band offsets determined in this work via XPS ($\Delta E_V = 0.56$ eV; $\Delta E_C = 1.25$ eV), one can find that the first-principles calculations suggest an empirical diffusion window of up to two monolayers. This is in excellent agreement with the experimentally determined diffusion window for Ge/AlAs(001) heterointerfaces as demonstrated by atom probe tomography analysis, which was found to be ∼6 Å (approximately two monolayers).[54] Moreover, the predominance of As−Ge bonds within the mixed monolayers is supported by the epitaxy conditions utilized herein, wherein an As_2 overpressure was maintained post-III−V growth and prior to wafer transfer into the isolated Ge epitaxy chamber (see Materials and Methods for additional growth details). Furthermore, investigations into the thermodynamic stability and formation energies of As−Ge and Al−Ge bonds in Ge and AlAs materials[35] indicate that under the vast majority of epitaxy conditions, As−Ge bonds exhibit lower formation energies than Al−Ge bonds and are thus more likely to form. Additionally, for the case of As-rich growth conditions, the As−Ge bond formation energy remains negative, suggesting the spontaneous formation of As−Ge bonds under thermodynamic equilibrium. This finding has important consequences for the design of future ε-Ge/$In_xAl_{1-x}As$ heterostructure-based optical devices, as it has been previously shown that a negative linear relationship exists between the As(V) diffusion length and ΔE_V.[35] Likewise, a similar relationship exists between increasing As content in the mixed As_bGe_{1-b} monolayer, that is, as the mixed monolayer becomes more As-rich, the corresponding heterointerfacial ΔE_V decreases.[54] As such, the synthesis of experimental and theoretical findings herein indicates that careful control over stressor (III−V) atomic diffusion into the overlying Ge epilayer is of utmost importance to maintain sufficient carrier confinement and functioning optical devices.

CONCLUSIONS

Our experimental results demonstrate that highly tensile-strained Ge epilayers can be realized on large-bandgap (e.g., $In_xAl_{1-x}As$) metamorphic buffers while maintaining coherent, atomically abrupt heterointerfaces. Key to accomplishing this is careful control over the growth temperature and growth rate, wherein low growth temperatures and rates allow for the minimization of both atomic interdiffusion and relaxation of the epitaxially induced lattice stress. Following these measures, we demonstrated an ∼1.75% biaxial tensile stress in an overlying Ge epilayer grown atop an $In_{0.26}Al_{0.74}As$ stressor. HR-XRD, TEM, and Raman spectroscopy were used to verify the epilayer crystallinity, heterointerface long- and short-range uniformity, and strain state of the Ge thin-film. Likewise, AFM demonstrated smooth surface morphologies (rms roughness ∼3.6 nm) and the development of a uniform, cross-hatched surface; the latter of which was indicative of symmetric metamorphic buffer relaxation, mirroring the HR-XRD results. Employing X-ray photoemission spectroscopy analysis, valence and conduction band offsets ($\Delta E_V = 0.56 \pm 0.1$ eV and $\Delta E_C = 1.25 \pm 0.1$ eV) were determined to project the extent to which large-bandgap $In_xAl_{1-x}As$ confines carriers to the ε-Ge epilayer. Moreover, a comparison of these findings with first-principles calculations of the ε-Ge/$In_xAl_{1-x}As$ interfacial electronic structure not only validated the empirical band alignment results, but also highlighted the critical role heterointerface

https://doi.org/10.1021/acsomega.1c06203
ACS Omega 2022, 7, 5946−5953

stoichiometry plays in determining band offsets and the need to control interfacial atomic species diffusion.

More generally, our results demonstrate how the atomic structure at the Ge/III−V heterointerface can be engineered to realize a wide range of energy band alignments. Selective termination of the III−V stressor surface, that is, with either group III or group V atoms, is expected to have a substantial impact on valence and conduction band offsets.[31,35,54] However, great care must be taken during crystal growth to control heterointerface interatomic diffusion and prevent the unintentional transition from one band alignment type to another (e.g., straddling to staggered). This is particularly important when designing photonic structures in which optical and electrical confinements are critical to device operation. Correspondingly, these results provide a unique pathway for the realization of group IV-based optoelectronic and photonic devices.

MATERIALS AND METHODS

Material Synthesis. The unintentionally doped ε-Ge epilayers studied in this work were grown using an in situ, dual-chamber MBE growth process leveraging separate III−V (composite) and group IV semiconductor growth reactors connected via an ultrahigh vacuum transfer chamber. The isolation of each growth phase is expected to minimize the likelihood of atomic interdiffusion at the ε-Ge/$In_xAl_{1-x}As$ heterointerface during subsequent epitaxy of the ε-Ge epilayer following $In_xAl_{1-x}As$ stressor growth. Reflection high-energy electron diffraction was used to analyze epilayer surface reconstruction at key points throughout the surface cleaning and subsequent heterostructure growth. A (001)GaAs substrate offcut 2° toward the ⟨110⟩ direction was first desorbed of native oxide at 750 °C under an arsenic (As_2) overpressure of ∼10^5 Torr as supplied by a valved As cracking source. It should be noted that substrate offcut has been previously demonstrated[55−59] to minimize the formation of antiphase domain boundaries during polar-on-non-polar epitaxy. As the ε-Ge/$In_{0.26}Al_{0.74}As$ heterojunction investigated herein was envisioned as a double heterojunction (i.e., $In_xAl_{1-x}As$/ε-Ge/$In_xAl_{1-x}As$) in practical (future) applications, this work utilized offcut (001)GaAs substrates to expand the applicability of the results. Following oxide desorption, 0.25 μm of homoepitaxial GaAs was grown at 660 °C, after which an ∼0.9 μm graded $In_xA_{l-x}As$ metamorphic buffer was grown at 420 °C to balance the dissimilar add-atom mobilities of indium (In) and aluminum (Al) surface dimers. After $In_xAl_{1-x}As$ buffer growth, a 15 min, 540 °C annealing step was introduced to provide sufficient thermal energy for the annihilation of in-grown dislocations resulting from the large lattice mismatch between the active region and substrate. An ∼0.6 μm constant-composition $In_xAl_{1-x}As$ (x_{exp} ∼ 0.26) stressor was then grown at 525 °C, after which the sample was cooled (under a decreasing As_2 overpressure) and transferred to the group IV reactor for Ge growth. During cooling of the sample following $In_xAl_{1-x}As$ virtual substrate epitaxy, the As needle valve was closed at a rate of ∼10% every 25 °C. As such, the low temperature at which the As_2 supply was terminated (∼275 °C) ensures that the III−V surface is As-terminated. A 10 nm-thick Ge epilayer was then grown at 400 °C using a growth rate of ∼0.067 Å/s to maintain an abrupt heterointerface. Following Ge epilayer growth, the sample was gradually cooled to ∼25 °C using a low 5 °C/min ramp rate to prevent the formation of defects because of the dissimilar thermal expansion coefficients between each epilayer.

Materials Characterization. The heterostructure crystal quality, $In_xAl_{1-x}As$ stressor composition, and epilayer relaxation and strain states were characterized using HR-XRD. X-ray rocking curves (i.e., ω-2θ scans) and RSMs were recorded using a PANalytical X-pert Pro system equipped with PIXcel and proportional detectors and a monochromatic Cu Kα (λ = 1.540597 Å) X-ray source. Analysis of the diffraction data was performed following the methods introduced in ref 38. Independent corroboration of the ε-Ge strain state was provided by Raman spectra collected in the (001) back-scattering geometry. All Raman spectra were captured using a JY Horiba LabRam HR800 system equipped with a 514.32 nm Ar laser source and calibrated using the Si LO mode at ω_0 ∼ 520 cm^{-1}. The surface morphology of the as-grown ε-Ge/$In_xAl_{1-x}As$ heterostructures was investigated using a Bruker Dimension Icon AFM in tapping mode. Finally, high-resolution cross-sectional transmission electron microscopy was performed on a JEOL 2100 TEM to study the structural quality, ε-Ge/$In_xAl_{1-x}As$ heterointerface uniformity, and lattice coherence of the strained layer/stressor heterointerface. The requisite electron transparent foils were prepared via standard polishing techniques, that is, mechanical grinding, dimpling, and subsequent Ar^+ ion beam milling at low temperature (∼150 K) to prevent the redeposition of the milled material on the imaging surface.

Heterostructure Band Alignment Characterization. The band alignment between the ε-Ge epilayer and the $In_{0.26}Al_{0.74}As$ stressor was investigated using a PHI Quantera SXM XPS system with a monochromatic Al Kα (E = 1486.7 eV) X-ray source. A low-energy electron flood gun was utilized to compensate positive charge accumulation in the samples because of photoelectron generation during sample X-ray irradiation. All CL and valence band binding energy spectra were collected with a pass energy of 26 eV and an exit angle of 45°. Correction for residual surface charging on each sample surface was performed by adjusting the experimental carbon 1 s CL peak position to the literature value of 285.0 eV. Curve fitting of the recorded spectra was performed using CasaXPS v2.3.14 utilizing Lorentzian peak shapes convolved over a Shirley-type background. The CL energy position was defined to be the center of the peak width at half the peak height (i.e., the FWHM). Additionally, the VBM for each bulk-like semiconductor was determined using a linear extrapolation of the onset of valence band photoemission. Finally, statistical deviation in the Au $4f_{7/2}$ CL binding energy of an Au standard was used to derive an experimental uncertainty of ±0.04%, wherein subsequent uncertainty was estimated using a root-sum-square approach.

AUTHOR INFORMATION

Corresponding Author

Mantu K. Hudait − *Advanced Devices and Sustainable Energy Laboratory (ADSEL), Bradley Department of Electrical and Computer Engineering, Virginia Tech, Blacksburg, Virginia 24061, United States;* orcid.org/0000-0002-9789-3081; Phone: +1 540 231 6663; Email: mantu.hudait@vt.edu; Fax: +1 540 231 3362

Authors

Michael B. Clavel − *Advanced Devices and Sustainable Energy Laboratory (ADSEL), Bradley Department of Electrical and*

https://doi.org/10.1021/acsomega.1c06203
ACS Omega 2022, 7, 5946−5953

Computer Engineering, Virginia Tech, Blacksburg, Virginia 24061, United States; orcid.org/0000-0002-2925-6099

Jheng-Sin Liu − *Advanced Devices and Sustainable Energy Laboratory (ADSEL), Bradley Department of Electrical and Computer Engineering, Virginia Tech, Blacksburg, Virginia 24061, United States*

Robert J. Bodnar − *Fluids Research Laboratory, Department of Geosciences, Virginia Tech, Blacksburg, Virginia 24061, United States*

Complete contact information is available at: https://pubs.acs.org/10.1021/acsomega.1c06203

Author Contributions

M.K.H. and M.B.C. conceived the research and performed the epitaxial heterostructure growths. M.B.C. and J.-S.L. performed the materials characterization and analysis, including the XRD, Raman, AFM, and TEM characterization. M.B.C. performed the XPS measurements and analysis. M.K.H. and R.J.B. supervised the research. All authors discussed the results and contributed to the writing of the manuscript.

Notes

The authors declare no competing financial interest.

■ ACKNOWLEDGMENTS

M.B.C. and J.-S.L. acknowledge partial support from the National Science Foundation under grant number ECCS-1507950 and ECCS-2042079, a US-Ireland joint R&D program. The authors would also like to acknowledge the Institute for Critical Technology and Applied Science's Nanocharacterization and Fabrication Laboratory and Virginia Tech Nanofabrication for access to their respective characterization facilities. M.B.C., M.K.H., and R.J.B. additionally acknowledge Charles Farley for assistance in performing Raman spectroscopy measurements. Finally, the authors are deeply grateful to Prof. Luke Lester for his helpful insights and discussions pertaining to strained Ge-based photonics.

■ REFERENCES

(1) Miller, D. A. B. Physical Reasons for Optical Interconnection. *Int. J. Optoelectronics* **1997**, *11*, 155−168.
(2) Miller, D. A. B. Device Requirements for Optical Interconnects to Silicon Chips. *Proc. IEEE* **2009**, *97*, 1166−1185.
(3) Herve, P.; Ovadia, S. Optical Technologies for Enterprise Networks. *Intel Technol. J.* **2004**, *8*, 73−82.
(4) Soref, R. The Past, Present, and Future of Silicon Photonics. *IEEE J. Sel. Top. Quantum Electron.* **2006**, *12*, 1678−1687.
(5) Soref, R. Silicon Photonics: A Review of Recent Literature. *Silicon* **2010**, *2*, 1−6.
(6) Liang, D.; Bowers, J. E. Recent Progress in Lasers on Silicon. *Nat. Photonics* **2010**, *4*, 511−517.
(7) Zhou, Z.; Yin, B.; Michel, J. On-Chip Light Sources for Silicon Photonics. *Light: Sci. Appl.* **2015**, *4*, 1−13.
(8) Hirschman, K. D.; Tsybeskov, L.; Duttagupta, S. P.; Fauchet, P. M. Silicon-based Visible Light Emitting Devices Integrated into Microelectronic Circuits. *Nature* **1996**, *384*, 338−341.
(9) Geiger, R.; Zabel, T.; Sigg, H. Group IV Direct Band Gap Photonics: Methods, Challenges, and Opportunities. *Front. Mater.* **2015**, *2*, 1−18.
(10) Kasper, E.; Kittler, M.; Oehme, M.; Arguirov, T. Germanium Tin: Silicon Photonics Toward the Mid-Infrared. *Photonics Res.* **2013**, *1*, 69−76.
(11) Liu, J. Monolithically Integrated Ge-on-Si Active Photonics. *Photonics* **2014**, *1*, 162−197.
(12) Dutt, B.; Sukhdeo, D. S.; Nam, D.; Vulovic, B. M.; Yuan, Z.; Saraswat, K. C. Roadmap to an Efficient Germanium-on-Silicon Laser: Strain versus N-type Doping. *IEEE Photonics J.* **2012**, *4*, 2002−2009.
(13) Li, X.; Li, Z.; Li, S.; Chrostowski, L.; Xia, G. Design Considerations of Biaxially Tensile Strained Germanium-on-Silicon Lasers. *Semicond. Sci. Technol.* **2016**, *31*, 065015-1−065015-9.
(14) Liu, J.; Sun, X.; Pan, D.; Wang, X.; Kimerling, L. C.; Koch, T. L.; Michel, J. Tensile-Strained, N-type Ge as a Gain Medium for Monolithic Laser Integration on Si. *Opt. Express* **2007**, *15*, 11272−11277.
(15) Bowers, J.; Liang, D.; Fang, A.; Park, H.; Jones, R.; Paniccia, M. Hybrid Silicon Lasers: The Final Frontier to Integrated Computing. *Opt. Photonics News* **2010**, *21*, 28−33.
(16) Fedeli, J.-M.; Ben Bakir, B.; Olivier, N.; Grosse, P.; Grenouillet, L.; Augendre, E.; Phillippe, P.; Gilbert, K.; Bordel, D.; Harduin, J. InP on SOI Devices for Optical Communication and Optical Network on Chip. *Proc. SPIE* **2011**, *7942*, 79420O.
(17) Duan, G.-H.; Jany, C.; Le Liepvre, A.; Accard, A.; Lamponi, M.; Make, D.; Kaspar, P.; Levaufre, G.; Girard, N.; Lelarge, F.; Fedeli, J.-M.; Descos, A.; Ben Bakir, B.; Messaoudene, S.; Bordel, D.; Menezo, S.; de Valicourt, G.; Keyvaninia, S.; Roelkens, G.; Van Thourhout, D.; Thomson, D. J.; Gardes, F. Y.; Reed, G. T. Hybrid III-V on Silicon Lasers for Photonic Integrated Circuits on Silicon. *Proc. SPIE* **2014**, *9002*, 90020X.
(18) Cai, Y.; Han, Z.; Wang, X.; Camacho-Aguilera, R. E.; Kimerling, L. C.; Michel, J.; Liu, J. Analysis of Threshold Current Behavior for Bulk and Quantum Well Germanium Laser Structures. *IEEE J. Sel. Top. Quantum Electron.* **2013**, *19*, 1901009.
(19) Sanchez-Perez, J. R.; Boztug, C.; Chen, F.; Sudradjat, F. F.; Paskiewicz, D. M.; Jacobson, R. B.; Lagally, M. G.; Paiella, R. Direct-Bandgap Light-Emitting Germanium in Tensilely Strained Nanomembranes. *Proc. Natl. Acad. Sci. U. S. A.* **2011**, *108*, 18893−18898.
(20) Jain, J. R.; Hryciw, A. C.; Baer, T. M.; Miller, D. A. B.; Brongersma, M. L.; Howe, R. T. A Micromachining-based Technology for Enhancing Germanium Light Emission *via* Tensile Strain. *Nat. Photonics* **2012**, *6*, 398−405.
(21) El Kurdi, M.; Prost, M.; Ghrib, A.; Elbaz, A.; Sauvage, S.; Checoury, X.; Beaudoin, G.; Sagnes, I.; Picardi, G.; Ossikovski, R.; Beouf, F.; Boucard, P. Tensile-Strained Germanium Microdisks with Circular Bragg Reflectors. *Appl. Phys. Lett.* **2016**, *108*, 091103-1−091103-5.
(22) Liu, J.; Sun, X.; Camacho-Aguilera, R.; Kimerling, L. C.; Michel, J. Ge-on-Si Laser Operating at Room Temperature. *Opt. Lett.* **2010**, *35*, 679−681.
(23) Camacho-Aguilera, R. E.; Cai, Y.; Patel, N.; Bessette, J. T.; Romagnoli, M.; Kimerling, L. C.; Michel, J. An Electrically Pumped Germanium Laser. *Opt. Express* **2012**, *20*, 11316−11320.
(24) Wirths, S.; Geiger, R.; von den Driesch, N.; Mussler, G.; Stoica, T.; Mantl, S.; Ikonic, Z.; Luysberg, M.; Chiussi, S.; Hartmann, J. M.; Sigg, H.; Faist, J.; Buca, D.; Grutzmacher, D. Lasing in Direct-Bandgap GeSn Alloy Grown on Si. *Nat. Photonics* **2015**, *9*, 88−92.
(25) Boucaud, P.; El Kurdi, M.; Sauvage, S.; de Kersauson, M.; Ghrib, A.; Checoury, X. Light Emission from Strained Germanium. *Nat. Photonics* **2013**, *7*, 162−163.
(26) Arguirov, T. V.; Kittler, M.; Oehme, M.; Abrosimov, N. V.; Vyvenko, O.; Kasper, E.; Schulze, J. Luminescence from Germanium and Germanium on Silicon. *Solid State Phenom.* **2014**, *205−206*, 383−393.
(27) Bai, Y.; Lee, K. E.; Cheng, C.; Lee, M. L.; Fitzgerald, E. A. Growth of Highly Tensile-Strained Ge on Relaxed $In_xGa_{1-x}As$ by Metal-Organic Chemical Vapor Deposition. *J. Appl. Phys.* **2008**, *104*, 084518-1−084518-9.
(28) Jakomin, R.; de Kersauson, M.; El Kurdi, M.; Largeau, L.; Mauguin, O.; Beaudoin, G.; Sauvage, S.; Ossikovski, R.; Ndong, G.; Chaigneau, M.; Sagnes, I.; Boucaud, P. High Quality Tensile-Strained N-doped Germanium Thin Films Grown on InGaAs Buffer Layers by Metal-Organic Chemical Vapor Deposition. *Appl. Phys. Lett.* **2011**, *98*, 091901-1−091901-3.

(29) Clavel, M.; Goley, P.; Jain, N.; Zhu, Y.; Hudait, M. K. Strain-Engineered Biaxial Tensile Epitaxial Germanium for High-Performance Ge/InGaAs Tunnel Field-Effect Transistors. *IEEE J. Electron Dev. Soc.* **2015**, *3*, 184−193.
(30) Hudait, M. K.; Clavel, M. B.; Lester, L.; Saladukha, D.; Ochalski, T.; Murphy-Armando, F. Heterogeneously Grown Tunable Group-IV Laser on Silicon. *Proc. SPIE* **2016**, *9755*, 97550Y-1−97550Y-11.
(31) Pavarelli, N.; Ochalski, T. J.; Murphy-Armando, F.; Huo, Y.; Schmidt, M.; Huyet, G.; Harris, J. S. Optical Emission of a Strained Direct-Band-Gap Ge Quantum Well Embedded Inside InGaAs Alloy Layers. *Phys. Rev. Lett.* **2013**, *110*, 177404-1−177404-5.
(32) Volodin, V. A.; Sokolov, L. V.; Pytyato, M. A.; Petikov, N. I.; Stoffel, M.; Rinnert, H.; Vergnat, M. Optical Properties of Tensile-Strained and Relaxed Ge Films Grown on InGaAs Buffer. *J. Appl. Phys.* **2014**, *115*, 053518-1−053518-6.
(33) Wang, K.; Gong, Q.; Zhou, H.; Kang, C.; Yan, J.; Liu, Q.; Wang, S. Mobility Enhancement in Tensile-Strained Ge Grown on InAlP Metamorphic Templates. *Appl. Surf. Sci.* **2014**, *291*, 45−47.
(34) Hudait, M. K.; Murphy-Armando, F.; Saladukha, D.; Clavel, M. B.; Goley, P. S.; Maurya, D.; Bhattacharya, S.; Ochalski, T. J. Design, Theoretical and Experimental Investigation of Tensile-Strained Germanium Quantum-Well Laser Structure. *ACS App. Electron. Mater.* **2021**, *3*, 4535−4547.
(35) Greene-Diniz, G.; Grüning, M. First-Principles Calculations of Band Offsets at Heterovalent ε-Ge/$In_xAl_{1-x}As$ Interfaces. *Phys. Rev. Appl.* **2018**, *10*, 044052-1−044052-16.
(36) Kim, J.; Fischetti, M. V. Electronic Band Structure Calculations for Biaxially Strained Si, Ge, and III−V Semiconductors. *J. Appl. Phys.* **2010**, *108*, 013710-1−013710-15.
(37) El Kurdi, M.; Fishman, G.; Sauvage, S.; Boucaud, P. Band Structure and Optical Gain of Tensile-Strained Germanium Based on a 30 Band ***k·p*** Formalism. *J. Appl. Phys.* **2010**, *107*, 013710-1−013710-7.
(38) Chauveau, J.-M.; Androussi, Y.; Lefebvre, A.; Di Persio, J.; Cordier, Y. Indium Content Measurements in Metamorphic High Electron Mobility Transistor Structures by Combination of x-ray Reciprocal Space Mapping and Transmission Electron Microscopy. *J. Appl. Phys.* **2003**, *93*, 4219−4225.
(39) Madelung, O. *Semiconductors: Intrinsic Properties of Group IV Elements and III-V, II-VI, and I-VII Compounds*; Springer: Berlin, 1985 Vol. *22a*.
(40) Goldman, R. S.; Wieder, H. H.; Kavanagh, K. L. Correlation of Anisotropic Strain Relaxation with Substrate Misorientation Direction at InGaAs/GaAs(001) Interfaces. *Appl. Phys. Lett.* **1995**, *67*, 344−346.
(41) Anastassakis, E.; Cardona, M. *High Pressure in Semiconductor Physics II*; Academic Press: San Diego, CA, 1998, Vol. *55*, Ch. 3.
(42) Clavel, M.; Saladukha, D.; Goley, P. S.; Ochalski, T. J.; Murphy-Armando, F.; Bodnar, R. J.; Hudait, M. K. Heterogeneously-Grown Tunable Tensile Strained Germanium on Silicon for Photonic Devices. *ACS Appl. Mater. Interfaces* **2015**, *7*, 26470−26481.
(43) Clavel, M. B.; Hudait, M. K. Band Offset Enhancement of a-Al_2O_3/Tensile Ge for High Mobility Nanoscale pMOS Devices. *IEEE Electron Device Lett.* **2017**, *38*, 1196−1199.
(44) Kraut, E. A.; Grant, R. W.; Waldrop, J. R.; Kowalczyk, S. P. Precise Determination of the Valence-Band Edge in x-ray Photoemission Spectra: Application to Measurement of Semiconductor Interface Potentials. *Phys. Rev. Lett.* **1980**, *44*, 1620−1623.
(45) Swaminathan, V.; MacRander, A. T. *Materials Aspects of GaAs and InP Based Structures*; Prentice Hall: Englewood Cliffs, NJ, 1991, Ch. 1.
(46) Brillson, L. J. *Surfaces and Interfaces of Electronic Materials*; Wiley: Weinheim, 2010, Ch. 20.
(47) Biasol, G.; Sorba, L.; Bratina, G.; Nicolini, R.; Franciosi, A.; Peressi, M.; Baroni, S.; Resta, R.; Baldereschi, A. Microscopic Capacitors and Neutral Interfaces in III-V/IV/III-V Semiconductor Heterostructures. *Phys. Rev. Lett.* **1992**, *69*, 1283−1286.
(48) Resta, R.; Baroni, S.; Baldereschi, A. Theory of Band Offsets at Semiconductor Heterojunctions: An *ab-initio* Linear Response Approach. *Superlattices Microstruct.* **1989**, *6*, 31−37.
(49) Van de Walle, C. G.; Martin, R. M. Theoretical Study of Band Offsets at Semiconductor Interfaces. *Phys. Rev. B: Condens. Matter Mater. Phys.* **1987**, *35*, 8154−8165.
(50) Franciosi, A.; Van de Walle, C. G. Heterojunction Band Offset Engineering. *Surf. Sci. Rep.* **1996**, *25*, 1−140.
(51) Yu, E. T.; McCaldin, J. O.; McGill, T. C. Band Offsets in Semiconductor Heterojunctions. *Solid State Phys.* **1992**, *46*, 1−146.
(52) Hybertsen, M. S. Role of Interface Strain in a Lattice-Matched Heterostructure. *Phys. Rev. Lett.* **1990**, *64*, 555−558.
(53) Zhu, Y.; Maurya, D.; Priya, S.; Hudait, M. K. Tensile-Strained Nanoscale Ge/$In_{0.16}Ga_{0.84}As$ Heterostructure for Tunnel Field-Effect Transistor. *ACS Appl. Mater. Interfaces* **2014**, *6*, 4947−4953.
(54) Clavel, M. B.; Greene-Diniz, G.; Grüning, M.; Henry, K. T.; Kuhn, M.; Bodnar, R. J.; Hudait, M. K. Engineering the Interfacial Electronic Structure of Epitaxial Ge/AlAs(001) Heterointerfaces via Substitutional Boron Incorporation: The Roles of Doping and Interface Stoichiometry. *ACS Appl. Electron. Mater.* **2019**, *1*, 2646−2654.
(55) Hudait, M. K.; Krupanidhi, S. B. Atomic Force Microscopic Study of Surface Morphology in Si-doped epi-GaAs on Ge Substrates: Effect of Off-Orientation. *Mater. Res. Bull.* **2000**, *35*, 909−919.
(56) Hudait, M. K.; Krupanidhi, S. B. Self-Annihilation of Antiphase Boundaries in GaAs Epilayers on Ge Substrates Grown by Metal-Organic Vapor-Phase Epitaxy. *J. Appl. Phys.* **2001**, *89*, 5972−5979.
(57) Takano, Y.; Masuda, M.; Kobayashi, K.; Kuwahara, K.; Fuke, S.; Shirakata, S. Epitaxial Growth of InGaAs on Misoriented GaAs(100) Substrate by Metal-Organic Vapor Phase Epitaxy. *J. Cryst. Growth* **2002**, *236*, 31−36.
(58) Ting, S. M.; Fitzgerald, E. A. Metal-Organic Chemical Vapor Deposition of Single Domain GaAs on Ge/Ge_xSi_{1-x}/Si and Ge Substrates. *J. Appl. Phys.* **2000**, *87*, 2618−2628.
(59) Hu, W.; Cheng, B.; Xue, C.; Su, S.; Liu, Z.; Li, Y.; Wang, Q.; Wang, L.; Liu, J.; Ding, J.; Lin, G.; Lin, Z. Epitaxy of $In_{0.01}Ga_{0.99}As$ on Ge/Offcut Si (001) Virtual Substrate. *Thin Solid Films* **2012**, *520*, 5361−5366.

https://doi.org/10.1021/acsomega.1c06203
ACS Omega 2022, 7, 5946−5953